2190 *Chem. Mater.* **2010,** *22,* 2190–2202
DOI:10.1021/cm9018474

CHEMISTRY OF MATERIALS
Article

Pt Alloy and Intermetallic Phases with V, Cr, Mn, Ni, and Cu: Synthesis As Nanomaterials and Possible Applications As Fuel Cell Catalysts

Tanushree Ghosh, Brian M. Leonard, Qin Zhou, and Francis J. DiSalvo*

Department of Chemistry and Chemical Biology, Cornell University, Ithaca, New York 14853

Received June 28, 2009. Revised Manuscript Received February 15, 2010

Nanomaterials as catalysts for fuel cells are not only highly desirable, but necessary to reach the high reaction rates (or power densities) demanded by many applications. The exploration of catalyst materials beyond Pt metal, such as Pt containing alloys and intermetallics, immediately leads to significant synthetic challenges to prepare nanoparticles with controlled composition, structure, and morphology. To facilitate a comprehensive study of these materials, a generalized synthetic approach is desirable. This requires an in-depth understanding and control of relevant factors that thermodynamically and kinetically define the synthesis process. Once synthesized, electrochemical activities of these materials can then be studied to aid in designing the next steps in further optimizing the catalyst activity. In this work, we have been able to demonstrate synthesis of several phases (both alloy and ordered intermetallics for binary Pt−V/Mn/Cr/Ni/Cu systems) that rarely, if ever, have been synthesized as nanomaterials without using surfactants. Additionally, we have shown that some of these materials are active catalysts, with activity superior to Pt for formic acid oxidation. Finally, we have established general guidelines and methodologies for synthesis of alloy and intermetallic phases as nanomaterials with highly reactive metals like Cr, V, and Mn.

Introduction

Developing sustainable energy technologies is important to reducing dependence on fossil fuels and to addressing environmental issues as well as global climate change. However, development of new, more affordable, durable, and efficient materials remains the key issue in advancing most of these technologies, particularly for fuel cells. While the efficiency of a fuel cell can in principle approach 100% of the free energy of reaction, only 50−60% efficiencies have been attained in hydrogen based fuel cells operating near room temperature at reasonable power densities.[1,2] That reduction in efficiency is due primarily to the slow kinetics of oxygen reduction at the cathode catalyst. While high anode efficiencies can be obtained for the oxidation of clean hydrogen on a Pt catalyst, impurities like CO and S, even in trace amounts (10 ppm CO, 1 ppb S) can poison the Pt catalyst. Because efficient and low cost generation and storage of clean hydrogen remains a challenge, current hydrogen fuel cells need to be accompanied either with reforming units, or hydrogen gas storage tanks, which typically have low volumetric energy densities, about 10 times lower than gasoline.[3] These issues have encouraged the consideration of fuels other than hydrogen, such as small molecules like formic acid and methanol as possible alternatives; however, slow oxidation kinetics and catalyst poisoning at the anode reduce the efficiencies of these simple carbon containing fuels.[4] These issues could possibly be addressed by designing more effective catalysts that are tolerant to typical poisons.

In order to improve both cost and activity, alloying Pt with a non-noble metal has proved to be a successful strategy for the development of new catalysts for methanol and other small molecule oxidation. CO is often an intermediate in these oxidative processes and causes catalyst poisoning by adhering to a pure Pt surface. A second metal can provide oxygenated species at lower potentials for the oxidative removal of the adsorbed CO. Pt alloys of Ru, Os, Sn, W, Mo, Co, Ni, etc. have been investigated, of which Pt−Ru (1:1) alloys have been found to be the most active and are current commercially used catalyst in Direct Methanol Fuel Cells (DMFCs).[4−8] The mechanism of activity and even the exact form and surface composition of the most active alloy catalyst are

*Corresponding author. E-mail: fjd3@cornell.edu.

(1) *Direct Methanol Fuel Cells: From a Twentieth Century Electrochemist's Dream to a Twenty-first Century Emerging Technology*; Lamy, C. L., Leger, J. M., Srinivasan, S., Ed.; Kluwer Academic/Plenum: New York, 2001; Vol. *34*.
(2) Shah, R. K.; K., S. J. *AES* (*Am. Soc. Mech. Eng.*) **2003**, 538.
(3) Schlapbach, L.; Zuttel, A. *Nature* **2001**, *414*, 353–358.
(4) Liu, H. S.; Song, C. J.; Zhang, L.; Zhang, J. J.; Wang, H. J.; Wilkinson, D. P. *J. Power Sources* **2006**, *155*, 95–110.
(5) Schmidt, T. J.; Gasteiger, H. A.; Behm, R. J. *Electrochem. Commun.* **1999**, *1*, 1–4.
(6) Narayanan, S. R.; Chun, W.; Valdez, T. I.; Jeffries-Nakamura, B.; Frank, H.; Surampudi, S.; Halpert, G.; Kosek, J.; Cropley, C.; LaConti, A. B.; Smart, M.; Wang, Q. J.; Prakash, G. S.; Olah, G. In *Fuel Cell Seminar*; Orlando, FL, November 17−20, 1996; Abstracts p 525.
(7) Antolini, E.; Salgado, J. R. C.; Gonzalez, E. R. *Appl. Catal., B* **2006**, *63*, 137–149.
(8) Costamagna, P.; Srinivasan, S. *J. Power Sources* **2001**, *102*, 242–252.

Published on Web 03/12/2010

still controversial.[5,9−12] This alloying approach is also relevant to oxygen reduction as some of these materials are promising cathode catalysts when they are coated with a monolayer of Pt to form core−shell nanoparticles.[13]

In the recent past, we successfully demonstrated the enhanced catalytic properties of ordered intermetallic nanomaterials (PtPb and Pt_3Ti) for formic acid and methanol oxidation.[14−17] Although synthesis of some alloy phases as nanoparticles has been demonstrated successfully by many researchers,[18−20] the synthesis of ordered intermetallic phases as nanomaterials has only recently begun to be systematically explored.[21−23]

Further investigation of these Pt−M intermetallic phases is important for several reasons. First, we had already explored Pb and Ti,[14,16,17] two very different metals in terms of reactivity with oxygen or water, and it was of interest to extrapolate the results to metals in between. Second, our collaborators are pursuing combinatorial thin film studies to identify potential binary, ternary, and quaternary catalyst compositions of Pt combined with metals from across the periodic table. Once electrochemically active compositions are identified, we need to know how to synthesize these phases as compositionally and structurally identical nanoparticles for testing their catalytic activity.

However, studying these and other intermetallic compounds as catalyst materials is quite challenging as many of them are extremely difficult to synthesize as clean nanoparticles. Most synthesis strategies to prepare nanosized intermetallic phases involve the use of surfactants. For catalyst applications in fuel cells, avoiding or subsequent removal of surfactants by thermal, chemical, or electrochemical treatment is crucial, since they block access of the reactants to the catalyst surface. High temperature processing may remove some surface contaminants, but will also result in agglomeration, particle size growth, and pyrolysis of contaminants making them more difficult to remove. These lead to a loss of active surface area and subsequently lower rates of reaction per unit mass of the catalyst.

Since there are many more compositions that need to be explored in the search for even better catalysts, identifying the key challenges associated with synthesizing intermetallic nanoparticles is vital. By understanding the key issues, we can develop a materials general synthesis for intermetallic nanoparticles allowing us to study them in more depth as catalysts for fuel cells

In our previous work with PtPb, we have shown that the identity of ligands and anions in the metal precursors play an important role in synthesizing homogeneous products and in determining particle size and surface composition, which in turn effect the catalytic activity.[24] Additionally, we have shown that under optimal conditions atomically ordered PtPb intermetallic nanoparticles could be prepared at room temperature without heating/annealing.[24] These studies allowed us to identify the general issues associated with solution phase synthesis of intermetallic nanoparticles (Supporting Information Scheme 1).[24]

However, on moving away from Pb, toward more electropositive and oxophilic elements, many of the interactions between the reduced metals and other components in the solvent (including the solvent itself) become larger. It was recognized that oxophilicity (affinity for oxygen) of the non-Pt element plays a central role in determining the nature and extent of these interactions. The selection of precursors for both metals thus becomes a critical issue. Wash solvents used after reduction also have to be selected much more carefully. At first we hypothesized that the differences in reduction potentials of the different metals played the deciding role, since simultaneous coreduction with Pt is important. However, we have found that strong reducing agents, such as sodium naphthalide, can address the coreduction issue as it was found to reduce nearly all elemental precursors (from group IV and beyond) instantaneously.

In this paper, we outline and discuss the key issues discovered as we investigated the challenges in synthesizing alloy and intermetallic nanoparticles, especially those that contain very electropositive metals such as Cr, Mn, and V. We first explored the reduction of single metals (Cu, Ni, Cr, and Mn—in the order of increasing electropositivity) using sodium naphthalide as a reducing agent (discussed in the Supporting Information section) and then explored the coreduction of these metals with Pt. We have successfully synthesized Pt_3V, Pt_3Cr, Pt_3Mn, PtNi, and PtCu ordered intermetallic nanoparticles and alloy nanoparticles in each of these systems. We detail the most successful synthetic routes obtained so far to prepare these alloy and intermetallics as nanometer size particles and also discuss future modifications for further control

(9) Gasteiger, H. A.; Markovic, N. M.; Ross, P. N. *J. Phys. Chem.* **1995**, *99*, 8290–8301.
(10) Casado-Rivera, E.; Gal, Z.; Angelo, A. C. D.; Lind, C.; DiSalvo, F. J.; Abruna, H. D. *Chemphyschem* **2003**, *4*, 193–199.
(11) Long, J. W.; Stroud, R. M.; Swider-Lyons, K. E.; Rolison, D. R. *J. Phys. Chem. B* **2000**, *104*, 9772–9776.
(12) Rolison, D. R.; Hagans, P. L.; Swider, K. E.; Long, J. W. *Langmuir* **1999**, *15*, 774−779.
(13) Adzic, R. R.; Zhang, J.; Sasaki, K.; Vukmirovic, M. B.; Shao, M.; Wang, J. X.; Nilekar, A. U.; Mavrikakis, M.; Valerio, J. A.; Uribe, F. *Top. Catal.* **2007**, *46*, 249–262.
(14) Alden, L. R.; Roychowdhury, C.; Matsumoto, F.; Han, D. K.; Zeldovich, V. B.; Abruna, H. D.; DiSalvo, F. J. *Langmuir* **2006**, *22*, 10465–10471.
(15) Matsumoto, F.; Roychowdhury, C.; DiSalvo, F. J.; Abruna, H. D. *J. Electrochem. Soc.* **2008**, *155*, B148–B154.
(16) Roychowdhury, C.; Matsumoto, F.; Zeldovich, V. B.; Warren, S. C.; Mutolo, P. F.; Ballesteros, M.; Wiesner, U.; Abruna, H. D.; DiSalvo, F. J. *Chem. Mater.* **2006**, *18*, 3365–3372.
(17) Abe, H.; Matsumoto, F.; Alden, L. R.; Warren, S. C.; Abruna, H. D.; DiSalvo, F. J. *J. Am. Chem. Soc.* **2008**, *130*, 5452–5458.
(18) Cable, R. E.; Schaak, R. E. *Chem. Mater.* **2005**, 17.
(19) Cable, R. E.; Schaak, R. E. *J. Am. Chem. Soc.* **2006**, *128*, 9588–9589.
(20) Schaak, R. E.; Sra, A. K.; Leonard, B. M.; Cable, R. E.; Bauer, J. C.; Han, Y. F.; Means, J.; Teizer, W.; Vasquez, Y.; Funck, E. S. *J. Am. Chem. Soc.* **2005**, *127*, 3506–3515.
(21) Maksimuk, S.; Yang, S.; Peng, Z.; Yang, H. *J. Am. Chem. Soc.* **2007**, *129*, 8684–8685.
(22) Wang, J.; Asmussen, R. M.; Adams, B.; Thomas, D. F.; Chen, A. *Chem. Mater.* **2009**, *21*, 1716–1724.
(23) Wang, J.; Holt-Hindle, P.; Macdonald, D.; Thomas, D. F.; Chen, A. *Electrochim. Acta* **2008**, *53*, 6944–6952.
(24) Ghosh, T.; Matsumoto, F.; McInnis, J.; Weiss, M.; Abruna, H. D.; DiSalvo, F. *J. Nanopart. Res.* **2009**, *11*, 965–980.

Table 1. Summary of Different Reactions Attempted to in Order to Understand and Achieve Coreduction of Different Metals with Pt[a]

metals	precursors (and other reagents)	reaction conditions
Pt−Cu	$Pt(acac)_2$, $Cu(acac)_2$	in THF, 10% excess of NaNp, stirred at room temperature for 3 h
Pt−Ni	$Pt(acac)_2$, $Ni(acac)_2$	in diglyme, 50% excess of NaNp, stirred at 120 °C for 3 h
	$Pt(acac)_2$, $Ni(acac)_2$	in THF, 10% excess of NaNp, stirred at room temperature overnight
	$Pt(acac)_2$, $Ni(acac)_2$	in THF, 100% excess of NaNp, stirred at room temperature for 5 days
	$Pt(acac)_2$, $Ni(acac)_2$, Vulcan	in THF, 10% excess of NaNp, 50 wt % loading of PtNi on Vulcan, stirred at room temperature for 4 h
	$Pt(acac)_2$, $Ni(acac)_2$, Vulcan	in THF, 10% excess of NaNp, 50 wt % loading of PtNi on Vulcan, stirred at room temperature for 5 days, precursors stirred with Vulcan in THF overnight before injection of reducing agent
Pt−Cr	$Pt(acac)_2$, $Cr(acac)_3$	in THF, 100% excess of NaNp, stirred at room temperature overnight
	$PtCl_2COD$, $CrCl_3$	in THF, 100% excess of NaNp, stirred at room temperature overnight
Pt−V	$PtCl_2COD$, VCl_2Cp_2	in THF, 100% excess of NaNp, stirred at room temperature overnight
	$PtCl_2COD$, VCl_3THF_3	in THF, 100% excess of NaNp, stirred at room temperature overnight
	$PtCl_2COD$, VCl_3	in THF, 100% excess of NaNp, stirred at room temperature overnight
Pt−Mn	$Pt(acac)_2$, $Mn(acac)_3$	in THF, 100% excess of NaNp, stirred at room temperature overnight
	$Pt(acac)_2$, $Mn(acac)_3$	in THF, 10% excess of NaNp, 50 wt % loading of PtNi on Vulcan, stirred at room temperature for 5 days, precursors stirred with Vulcan in THF overnight before injection of reducing agent

[a] The procedure described in the table for Pt−Cu was generally the method followed. However in some cases, minor variations were introduced and only those variations are specified in the table.

of particle size and composition. Once we were able to consistently synthesize these materials, we examined their electrocatalytic activity. Formic acid was chosen for examining the electrocatalytic activity, since use of this fuel often leads to CO poisoning, and we are searching for more poison tolerant catalysts.

Experimental Section

Materials. All reactants were used as received. Sodium metal, all solvents, and VCl_3THF_3 (THF = tetrahydrofuran) were purchased from Aldrich. Naphthalene was purchased from Fisher. All other metal precursors were purchased from STREM Chemicals Inc. Methanol was degassed by bubbling Ar through the solution for 1 h prior to use, and all other solvents (THF, hexanes, and diglyme) were obtained from a solvent system (custom built Seca solvent system by Glass Contour). All reactants were stored in an argon atmosphere glovebox, and reactions were carried out either in the glovebox or on Schlenk lines without air exposure.

Sodium Naphthalide. Sodium naphthalide solutions were prepared in either THF or diglyme (bis(2-methoxyethyl)ether, MW = 134.18) according to well-known literature methods.[25] Stoichiometric amounts of naphthalene and sodium metal were weighed out in an argon atmosphere glovebox and added to a flask containing 40 mL of the solvent. The sealed flask was removed from the glovebox and stirred overnight under argon to produce a dark green sodium naphthalide solution.

Single Precursor Reductions with Sodium Naphthalide. A metal precursor solution ($Ni(acac)_2$,$Cr(acac)_3$, $Mn(acac)_3$, $Cu(acac)_2$, $CuCl_2$ or $Cu(C_2H_3O_2)_2$ where acac = acetylacetonate anion, $C_5H_7O_2^-$, 0.5 mmol in 20 mL THF) was injected into a flask containing a freshly prepared sodium naphthalide solution in THF maintaining a constant 10% excess of the reducing agent in all cases. The dark green sodium naphthalide solution immediately changed color to brown/black and was stirred for 3 h or overnight at room temperature. The reaction solution was centrifuged at 9000 rpm for 30 min to collect the reduced metal product, but typically little to no product would precipitate out of solution for these reactions. The solvent was then removed by vacuum distillation and the remaining solid product was collected and washed with hexanes and methanol to obtain the final product. After a final hexane wash, the tube was pumped to dryness, backfilled with argon and pumped into the argon atmosphere glovebox. Further details on the products obtained from these single element reductions are available in the Supporting Information.

Pt Alloys and Ordered Intermetallics. The general procedure followed for coreduction of metal precursors is discussed below. Table 1 gives a complete summary of all the different reactions carried out in order to understand and control coreduction, nucleation and growth of nanoparticles of different Pt containing alloys and ordered intermetallics.

Stoichiometric amounts (0.5 mmol each) of metal precursor pairs ($Mn(acac)_3$/$Pt(acac)_2$, $Ni(acac)_2$/$Pt(acac)_2$, $V(THF)_3Cl_3$/$PtCl_2COD$ (COD = 1,5 -cyclooctadiene, C_8H_{12}), $V(Cp)_2Cl_2$/$PtCl_2COD$ (Cp = cyclopentadienyl anion, $C_5H_5^-$), $Cr(acac)_3$/$PtCl_2COD$), $CrCl_3$/$PtCl_2(COD)$, $Cu(acac)_2$/$Pt(acac)_2$) were dissolved in 20 mL THF in a scintillation vial inside the argon atmosphere box. The solution was brought out of the glovebox in a syringe and quickly injected into a flask containing a freshly prepared dark green sodium naphthalide solution in THF. The reducing agent excess was maintained at 10%; however, in some cases mentioned below (see Table 1), a 100% reducing agent excess was used. Instantaneous color change from dark green to opaque dark brown/black was observed in every case. The solution was allowed to stir for 3 h. In a few initial reactions, the reaction mixture was transferred into a centrifuge tube and centrifuged (9000 rpm, 30 min) in effort to precipitate the product out of the reaction solvent. However, since no precipitate was observed (except for coreduction of $Pt(acac)_2$ and $Ni(acac)_2$, where some solid product was obtained), this step was omitted thereafter and the solvent was evaporated to dryness using a vacuum pump. The product was then washed with hexanes and methanol/hexanes mixtures in an attempt to remove the more polar byproducts. After a final hexane wash, the product was dried under vacuum, backfilled with argon, and slowly exposed to air by putting a needle through the septum (in previous work, it was observed that if the products were quickly exposed to air, they frequently "smoked" or burst into flame).[14] pXRD, EDS, electron microscopic imaging (SEM, STEM, TEM—dark field and bright field), and TGA measurements were carried out on these final (air exposed) products. Table 1 gives a summary of all the reactions carried out.

(25) Connelly, N. G.; Geiger, W. E. *Chem. Rev.* **1996**, *96*, 877–910.

Instrumentation. All powder X-ray diffraction (pXRD) scans were taken on a Scintag XDS 200 powder X-ray diffractometer using Cu Kα radiation. pXRD patterns taken under inert conditions were prepared by loading the sample onto a sample holder in an argon-filled glovebox and covering it with a mylar film before removing it from the glovebox for analysis. Thermal gravimetric analysis was performed on a TA Instruments Q50. The SEM and TEM imaging were obtained using a LEO-1550 Field Emission SEM (FE-SEM) and a TECNAI T-12 at 120 KV, respectively. For imaging purposes, a solution of nanoparticles was made by suspending the particles in 5 mL of degassed isopropyl alcohol and sonicating using a 3150 Bransonic ultrasonic cleaner. This solution was then dropped onto a carbon coated copper grid. For EDS measurements on the SEM, TEM, or STEM, samples were prepared by transferring dry powder onto 300 mesh copper grids in order to avoid possible reaction of the electropositive metal with isopropyl alcohol affecting the composition. To measure the surface area of the samples, a Micromeritics ASAP 2020 was used to collect a partial adsorption isotherm at liquid nitrogen temperature (−196 °C) with krypton or nitrogen as the adsorption gas over the pressure range (P/P_0) of 0.06−0.5. Prior to measurements, the sample was degassed under vacuum at room temperature for 48 h. The specific surface area was determined according to the Brunauer−Emmett−Teller (BET) method in the relative pressure (P/P_0) range of 0.08−0.185.

Electrocatalytic Activity. The electrocatalytic activity of the Pt−Cu, Pt−Ni, Pt−Cr, Pt−V, and Pt−Mn nanoparticles were tested for formic acid oxidation. Prior to each experiment, a suspension of the nanoparticle catalyst was prepared as follows: to 8 mg of the dried nanoparticle sample were added 3.98 mL of distilled water and 1 mL of isopropyl alcohol (Aldrich). Additionally, 20 μL of a 5% w/w Nafion solution in alcohols and water (Aldrich, EW: 1100) was added to this mixture. The resulting mixture was sonicated in a bath type ultrasonicator for 1 h. Each nanoparticle suspension described above was coated onto a 4 mm diameter glassy carbon (GC) electrode. The GC electrode had been previously polished with diamond paste (METADI-Buehler, ∅ = 1 μm) and ultrasonicated in Millipore water (18 MΩ cm^{-1}, Millipore Milli-Q) for 10 min. The electrode was then rinsed with Millipore water and allowed to dry in air. A 140 μg cm^{-2} portion of the nanoparticle (10.8 μL of nanoparticle suspension) was coated onto the clean GC electrode. The coated electrode was then dried in air.

Formic acid oxidation on the nanoparticle-coated GC electrode was examined in a mixture of 0.5 M formic acid (Mallinckrodt, 88% analytical reagent) and 0.1 M sulfuric acid. A three-electrode electrochemical cell was used for all electrochemical measurements. The reference electrode was a sodium chloride saturated Ag/AgCl electrode, and the counter electrode was a platinum coil. All electrochemical experiments were carried out at room temperature with a Pine AFRDE2 potentiostat. All solutions were prepared with Millipore water and deaerated with prepurified argon for at least 15 min before each experiment.

Results and Discussion

The goal of this work is to delineate factors that influence nanoparticle synthesis and to develop an understanding of, and possibly general guidelines for, solution phase syntheses of bimetallic nanoparticle phases by coreduction. To achieve this, it is vital to minimize the interfering effects of the byproduct, from both reducing agent and precursors and perhaps even the solvent so that the desired phases could be isolated from the reaction solvent. If the other species present in the solution do not interact strongly with the metal particles post-reduction, the desired bimetallic phases should be able to nucleate and possibly grow without in situ heating or post-reaction annealing. Additionally, the side products should be easily removed from the reaction solvent by washing, ultimately resulting in clean particle surfaces. Another concern when dealing with very electropositive metals is leaching from the surface.[26−30] If the particles are allowed to grow in the mother liquor to larger than 5 nm in diameter, removal of the more electropositive metal by reaction with methanol or by oxidation on exposure to air should occur only on the surface. It appears from our experiments that a strong association of the side products with the reduced metals keeps the intermetallic phases from nucleating/growing in situ. Such strong association is expected, since the binding energy of organic ligands, especially unsaturated species, with transition metal atoms and transition metal surfaces is known to be large, often 100 kJ/mol or more.[31−33] The structure and composition of the nanoparticles that are produced in this study by room temperature reduction cannot be unambiguously determined, since the nanoparticles are so small (X-ray diffraction peak widths are up to 10−20° wide). Due to the interaction of organic species with the metals, it is likely that the metal−metal bonds within such nanoparticles form a percolation[34] or dendritic network and that the bound organic species are both inside and on the surface of these nanoparticles. Scheme I (of the Supporting Information) outlines a possible kinetic pathway that illustrates these ideas. The inclusion of neutral and ionic bound species in the nanoparticles likely prevents the products from precipitating out of solution. Such open structures may allow diffusion of wash solvents or air into the structure which can result in significant loss of the electropositive metals during workup, as has been observed in the case of Pt−Ti.[17]

To address this challenge, two synthetic variables have been explored: the role of precursors in sodium naphthalide reduction reactions and the influence of both reaction and wash solvents. First we explored the role of the precursors since they produce a significant amount of the byproduct in the reaction. On the basis of our experience with very electropositive and oxophilic metals like Ti, we examined the effect of oxygen containing vs

(26) Pickering, H. W. *Corros. Sci.* **1983**, *23*, 1107.
(27) Erlebacher, J. *J. Electrochem. Soc.* **2004**, *151*, C614–C626.
(28) Erlebacher, J.; Aziz, M. J.; Karma, A.; Dimitrov, N.; Sieradzki, K. *Nature* **2001**, *410*, 450–453.
(29) Rugolo, J.; Erlebacher, J.; Sieradzki, K. *Nat. Mater.* **2006**, *5*, 946–949.
(30) Sieradzki, K.; Dimitrov, N.; Movrin, D.; McCall, C.; Vasiljevic, N.; Erlebacher, J. *J. Electrochem. Soc.* **2002**, *149*, B370–B377.
(31) Tsai, Y.-L.; Koel, B. E. *J. Phys. Chem. B* **1997**, *101*, 2895–2906.
(32) Salmeron, M.; Somorjai, G. A. *J. Phys. Chem.* **1982**, *86*, 341–350.
(33) Gottfried, J. M.; Vestergaard, E. K.; Bera, P.; Campbell, C. T. *J. Phys. Chem. B* **2006**, *110*, 17539–17545.
(34) Zallen, R. *Physics of Amorphous Solids*; Wiley Interscience: New York, 1983.

oxygen free precursors and used that as a tool in controlling the final composition for the highly oxophilic metals.

Our choice of precursors is also limited by other factors. Sodium naphthalide is compatible with only ethereal or glyme solvents, limiting our precursor choice to those with at least moderate solubility in these solvents. Metal chlorides and many organometallic compounds often have low or negligible solubility in ethers, however, precursors with both chloride and neutral or anionic organic ligands (e.g., $V(Cp)_2Cl_2$ or $Ti(THF)_3Cl_3$) are often suitable, as are metal acetylacetonates and ethylhexanoates (e.g., $Cr(2\text{-ethylhexanoate})_3$). Generally, precursor metals in their highest oxidation state are preferred to prevent internal redox reactions when the precursors are mixed, since this may lead to precipitation of one of the metals prior to addition of the reducing agent, resulting in a mixed phase product.[35]

A second consideration is solvent choice and its ability to remove the side products without affecting the reactive metal. By precipitating the product from the reaction or wash solvent, the side products are left in solution with few species bound to the nanoparticle surface. These surface bound species could possibly be removed by repeated washings or by low temperature sublimation. As described earlier, this would only be possible if these side products are not too strongly bound to the reduced metals. To better understand the nature of the association of these species to the metals, we attempted to simplify the reactions and compare single metal reductions, with smaller amounts of excess reducing agent. For this reason, metal acetylacetonates were the precursors chosen for most of these studies, since they are readily available, soluble, and, even for the wide range of metals studied, only one anionic ligand is needed. Thus it is possible to directly study the role of the different metals themselves in determining the course of the reactions. The phenomenon of ligands contaminating the nanoparticle surface and their role in determining nanoparticle domain size and their electrochemical properties has been well-studied in the PtPb system.[24] To confirm and extrapolate our understanding to the case of metals more electrophilic than Pb, it is logical to first start by reducing that metal by itself. Our observations with PtPb suggested that products precipitated out the reaction solvent have less contamination than the products that were recovered by evaporation of the reaction solvent. As it can be concluded from combining these points, the objective in the single precursor reductions was to determine conditions under which the product could be isolated from the reaction solvent (THF) post-reduction.

Single Precursor Reductions. It is apparent even in the single precursor reductions that the byproduct remaining in the solution indeed play a significant role in determining the properties of the final product, such as nanoparticle size and precipitation behavior. The behavior of each metal is discussed in detail in the Supporting Information section in the order of increasing oxophilicity. Below, we discuss the key observation and inferences.

For copper, three different precursors ($Cu(acac)_2$, $CuCl_2$, and $Cu(C_2H_3O_2)_2$) were used to study the effect of ligands on the formation of nanoparticles. Cu was chosen because it is the least electropositive of those studied, and thus least reactive with solvents, water, and air once reduced. For all precursors, no solid precipitations was observed upon centrifuging, so the THF was evaporated off completely, and the product was worked up following the standard procedure described in the Experimental Section. No significant effect of the ligands could be inferred from these experiments with Cu as all products had comparable particle sizes (~2−3 nm) and behaved similarly in terms of precipitation. Thus for the other metals, only one type of precursor, acetylacetonate (acac) salts, was explored.

The product nanoparticles from single metal reduction remained very small (2 nm or less) for all the metals included in this study and were very difficult to precipitate from the solvent. In the case of oxophilic metals, the small particle size exacerbates the problem of the reactive metal being oxidized and solubilized by reacting with wash solvents such as methanol. For the single metal reactions, the solution was allowed to stir for 3−24 h, but upon centrifuging at 9000 rpm for 30 min, no products precipitated out for any of the metals (Ti, V, Cr, Mn, Ni, and Cu). Occasionally the metal nanoparticles would precipitate out upon vacuum removal of most of the THF, but typically the solutions were evaporated to dryness then worked up using a methanol/hexane wash. The products recovered from these single metal reactions were pumped into an argon filled glovebox and air free pXRD patterns were obtained. For all the metals, pXRD of the unannealed sample were inconclusive due to small particle size or amorphous/unclean materials coupled with a large background signal from the protective mylar film. However, on exposing these powders to air, the product quickly changed colors to something similar to the respective oxide phase; for example, the Mn product changed from a brown powder to a dark gray/green consistent with MnO or Mn_2O_3.

To obtain larger particles with sharper, more identifiable diffraction peaks, the Cu and Mn products were annealed in sealed, evacuated silica tubes to 600 °C, without exposing the sample to air. We believed that sufficient information could be obtained by annealing one more electropositive and one less electropositive metal product (Mn and Cu, respectively); therefore, Ni and Cr products were not annealed. In the case of Cu, the annealed product was well-crystallized (domain size greater than 18 nm) with X-ray diffraction peaks that matched the Cu pattern (for all Cu precursors reduced), with little or no copper oxides visible. For Mn, the annealed pXRD pattern had broad peaks near those expected for MnO. Even after repeated attempts only oxidized species could be obtained for highly reactive metals like Mn.

(35) Leonard, B. M.; Schaak, R. E. *J. Am. Chem. Soc.* **2006**, *128*, 11475–11482.

EDS confirmed the presence of sodium in all cases and weight loss was observed in TGA experiments corresponding to an organic residue being removed. Since Na(acac) by itself is soluble in THF, we concluded that acac must have some affinity for the neutral metal surfaces. These surface bound species curtail particle growth at room temperature, but not at elevated temperatures. Apparently these surface species also solubilize the small particles, preventing them from precipitating in THF, even under high speed centrifuging. Methanol/hexane washes were not sufficient to remove all the materials adhering to the nanoparticles, and thus, no specific trends with oxophilicity or electropositivity of the metals in terms of their precipitation behavior could be inferred.

Thus, in the absence of Pt, further characterization of most of the as-prepared elemental nanoparticles was not possible, due to the difficulty isolating these nanoparticles from solvent resulting in low yields (< 50%) and the high reactivity of isolated product with air.

Co Reduction with Platinum (Pt:M Reactants All with 1:1 Atomic Ratios). We hoped that the presence of a second metal like Pt would alter the affinity of the side products and thus the precipitation behavior of the particles so that the product could be easily obtained and characterized. We first discuss the observations for coreductions below, starting with the least reactive metal, Cu, followed by Ni, Cr, V, and Mn (in the order of increasing electropositivity, which is different than the order of oxophilicity, as Mn is more electropositive, but less oxophilic than Cr and V). Then, we outline the general guidelines (Selection of Precursors) and observations (presence of contaminants, and possible ways to generate cleaner particles) as discovered through these processes.

The synthesis and workup procedure followed for all metals were same (as described in the Experimental Section). However, the precursors were varied for some metals and annealing temperature and time was selected based on the system and composition detected by EDS to target the ordered phase closest to the composition as given by the system phase diagrams.[36]

Pt−Cu. The platinum copper system has a relatively low affinity for oxygen, reflected in the positive reduction potential of both metals and produces nanoparticles with good yield and relatively low temperature intermetallic formation. Acetylacetonate precursors were used for both the Pt and Cu sources due to enhanced solubility and little concern for the formation of copper oxides. Upon injection of the metal precursors, the solution immediately turns black indicating reduction of the metal ions. The 1:1 product did not precipitate out of the solution with centrifugation, so THF was removed by vacuum and the product was washed with hexanes followed by hexanes/methanol mixtures. The resulting black powder was dried under vacuum and exposed to air slowly overnight by inserting a needle through the septum. The as-made powder showed a shift in the X-ray diffraction pattern from that of Pt (most intense peak ~40° 2θ) to a smaller cubic lattice constant, consistent with significant alloying (Figure 1). Atomic ordering of the as-made sample could not be confirmed due to the small particle size that results in broad diffraction peaks. The as prepared sample of PtCu had the narrowest diffraction peaks of all the binary systems, yet confirmation of the ordered phase still could not be determined by X-ray or electron diffraction due to the line broadening that results from the small particle size. Annealing the powder at 250 °C caused some growth of the particle size from 6 to 14 nm as determined by the Scherrer equation, and the ordered intermetallic phase PtCu could then be observed by the superlattice peaks in the diffraction pattern. As seen by sharper diffraction lines, annealing the sample at higher temperatures caused more sintering and particle growth. In these experiments, no black film formed on the silica tube, even at 400 °C, indicating that little organic residue remained in the product. The PtCu system had the lowest weight loss (9%) and lowest intermetallic formation temperature of all the binary systems we studied. It is assumed that these two facts are connected and the lower intermetallic formation temperature is a result of weaker binding between the organic species present and the Pt/Cu surface. In our experience, only PtPb was found to behave similarly forming these condensed nanoparticles at room temperature or after annealing at low temperatures.[14,24] Figure 2 shows TEM images of the PtCu particles prior to annealing with small 3−5 nm particles, while the annealed sample shows some aggregation and sintering. Selected area electron diffraction (SAED) also shows a broad, diffuse diffraction pattern for the as prepared sample and sharper rings for the annealed sample, consistent with the pXRD data. EDS for both as-made and annealed samples confirmed the 1:1 composition (±5%).

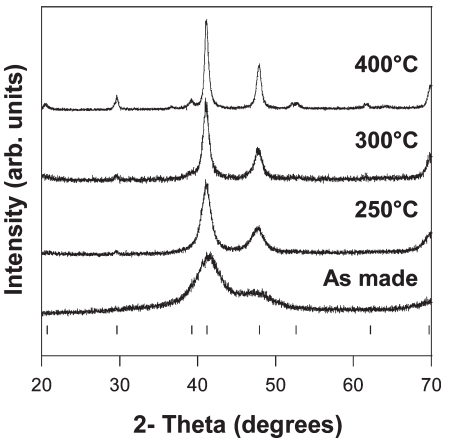

Figure 1. pXRD of PtCu nanoparticles as-made and annealed to 250, 300, and 400 °C. The as-made sample shows a significant shift from the Pt lattice due to the incorporation of Cu. Upon annealing the sample at 250 °C, the intermetallic phase is formed as seen by the weak ordering peaks at 20.7°, 29.6°, 52.6°, and 62.1° 2θ. Tick marks at the bottom indicate the expected peak positions for intermetallic PtCu (PDF no. 00-042-1326).

(36) *Desk handbook: Phase diagrams for binary alloys*; Illustrated ed.; Okamoto, H., Ed.; ASM International, 1990.

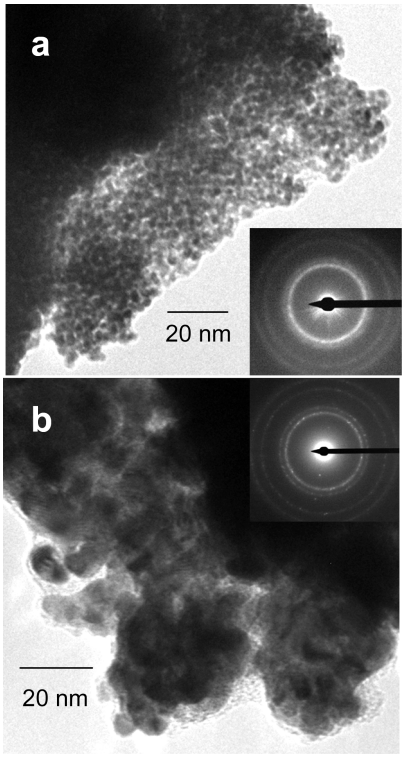

Figure 2. TEM images of PtCu nanoparticles (a) as synthesized and (b) after annealing at 250 °C. Electron diffraction is inset in each picture showing a diffuse cubic pattern for the as synthesized sample and more crystalline ordered tetragonal pattern for the annealed sample.

Pt−Ni:Ni has low oxophilicity and reduction potential (see Supporting Information Table S1) which is consistent our with single precursor reduction observations that show little/no reactivity with methanol. Thus, Ni was expected to coreduce with platinum in a manner similar to the Cu case above, to form the desired alloy and intermetallic phases. Acetylacetonate precursors were expected to be appropriate for the same reasons. However, as evident from the Pt−Ni phase diagram, the tetragonal intermetallic PtNi phase might be difficult to obtain since it exists only within a narrow range of temperature. The room temperature coreduction of platinum and nickel acetylacetonates with sodium naphthalide yields a final product of composition Pt:Ni of 1:0.6 ± 5% (atomic ratio). The average Ni content is a little low compared to the reactant ratio, even considering the semiquantitative nature of the EDS measurement; so some Ni might have reacted with methanol during the workup. pXRD of the room temperature sample suggested a cubic alloy phase of Pt with broad peaks that were shifted toward higher angles due to incorporation of Ni in the lattice. Annealing the product in a tube sealed under vacuum at 600 °C for 4 h gave single phase intermetallic with the PtNi structure and a 20.5 nm domain size as determined by the Scherrer equation and trace amounts of unknown impurities (Figure 3).

Annealing at a higher temperature for longer times (670 °C, 48 h) yielded predominantly the $Pt_{0.5}Ni_{0.5}$ alloy, which is to be expected based on the phase diagram. All the tubes used for annealing were coated with a black film, indicating that the sample contained some organic

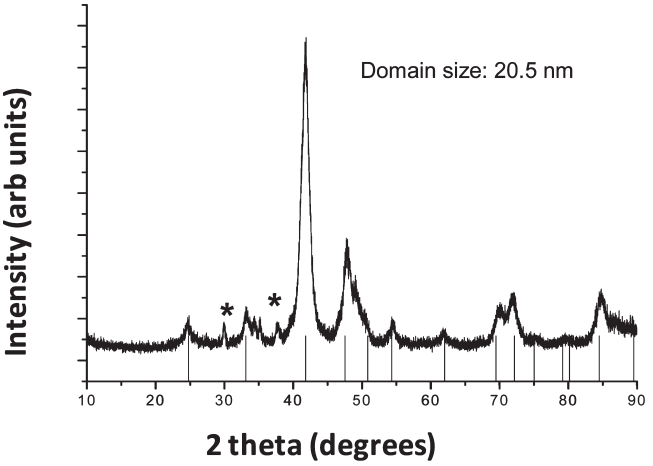

Figure 3. pXRD image of PtNi ordered tetragonal phase obtained by coreduction of $Pt(acac)_2$ and $Ni(acac)_2$, followed by annealing at 600 °C for 4 h. Tick marks represent the known peak positions for the PtNi tetragonal phase (PDF no. 03-065-9446). * = unknown impurity peaks.

species before heating. This is consistent with the larger weight loss (35%) on heating the products as observed by TGA.

Using the Pt−Ni as a model system, we tested the effects of changing reaction solvent, stirring time, and supporting the catalyst on Vulcan. First, we investigated changing the reaction solvent to diglyme and subsequent heating in the mother liquor. Heating to 120 °C in diglyme following injection of the Na naphthalide produced a large amount of precipitate on standing. However, some product could not be precipitated even in a centrifuge and could be recovered only by evaporating off the diglyme. The pXRD for the product that precipitated had many low intensity peaks which were difficult to index. The product collected from the supernatant showed very broad diffraction peaks, but on annealing (670 °C, 48 h), showed sharp peaks indexing on the tetragonal cell of the PtNi structure. EDS showed the composition to be Pt:Ni 1:0.7 ± 5% (atomic ratio).

Previous research in our group showed that stirring time is another important variable in intermetallic formation.[37,38] Consequently, in another reaction the product solution was allowed to stir for 5 days after reduction at room temperature to see if the particles might grow enough to precipitate from the solution. The product did not precipitate on standing, but did precipitate on centrifuging, in contrast to the behavior of the sample that was stirred for only 3 h. Nonetheless, the product was still an alloy phase as observed by broad X-ray diffraction peaks with no evidence of ordering in the pXRD pattern. On annealing (600 °C, 4 h), unlike the previous room temperature reaction, the cubic PtNi alloy and not the tetragonal intermetallic phase was obtained. Co-injection of the precursors into the reducing agent solution with Vulcan (to form supported Pt−Ni phases) was successful,

(37) Alden, L. R. Synthesis of platinum intermetallic compounds for fuel cell anode catalysts. Cornell University, 2006.
(38) Roychowdhury, C. Intermetallic nanoparticles for fuel cell applications: syntheses and characterization studies. Cornell University, 2008.

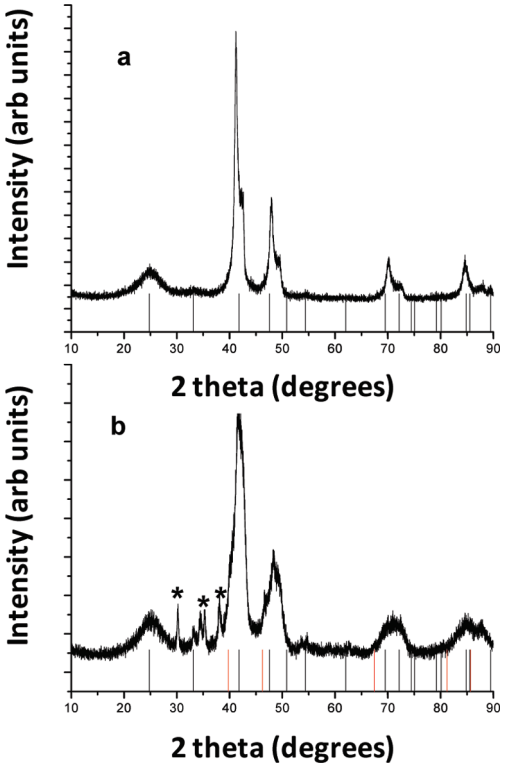

Figure 4. pXRD patterns of PtNi phases from coreduction of precursors in presence of C black (Vulcan) after annealing at (a) 800 and (b) 670 °C. Particle agglomeration and growth is significantly decreased in the presence of C support. * = unknown impurity peaks. Black tick marks represent the known peak positions for PtNi (PDF no. 03-065-2797). Red tick marks show 2θ positions for the Pt phase (PDF no. 04-001-2683).

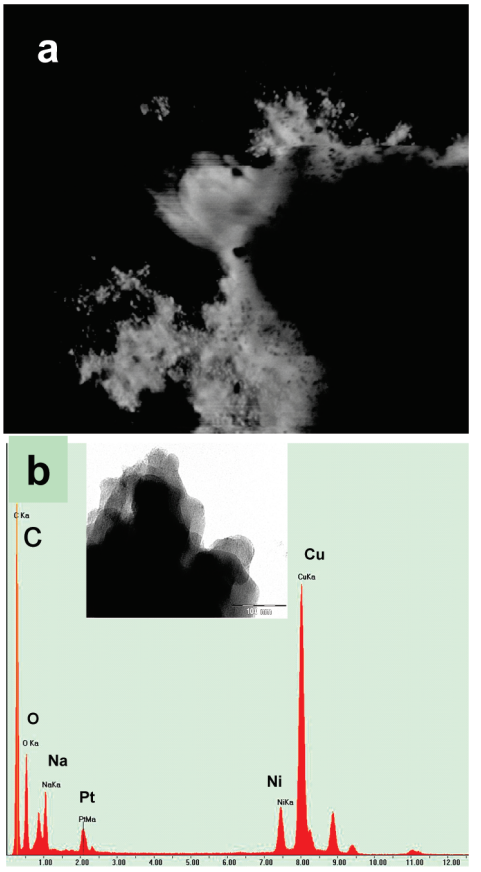

Figure 5. (a) Darkfield TEM image (full scale = 3 μm) and (b) plot showing high Z elements as white specks on the C support and EDS data of the PtNi obtained from coreduction of precursors in the presence of C black. The inset shows the region on which EDS data was obtained. The Cu signal comes from the TEM grid.

yielding a cubic PtNi alloy on annealing, but with much less particle size growth than the unsupported sample (8 vs 15 nm for unsupported). This can easily be seen by broader peaks in the pXRD data (Figure 4a and b), and smaller particles in the brightfield and darkfield TEM images (Figure 5a and b). Additionally, the supported particles can be precipitated out of polar solvents more easily than the unsupported product, which simplifies collecting and washing the product. Taken together, this demonstrates the ability of this synthetic method to produce bimetallic particles supported on carbon in a one pot reaction and maintains relatively small particles even after annealing at high temperatures.

Pt−Cr. In the case of coreduction of platinum and chromium acetylacetonates, the EDS data showed the composition of the product to be mostly Pt (Pt:Cr was about 8:1). Thus, oxygen free precursors were used in an attempt to increase the Cr content in the final product. $CrCl_3$ and $PtCl_2COD$ was the first oxygen-free precursor combination examined for Pt−Cr systems. Room temperature reduction yielded a product with a Pt:Cr atomic ratio of 1:0.8, and pXRD showed very broad peaks indexing close to cubic Pt, but shifted slightly toward higher angles. On annealing in a tube sealed under vacuum at 500 °C for 48 h or 800 °C for 24 h, cubic Pt−Cr alloy phases were obtained. However, annealing at 700 °C for 24 h gave the Pt_3Cr ordered intermetallic phase (Figure 6).

This indicates that some Cr is lost either in a second phase or by reaction with the methanol wash. Similar to the previous samples, all the annealing tubes were coated with a black film on the inside from the decomposition of organic species in the sample. Also, the pXRD showed the presence of significant amount of NaCl, which are expected in cases where chloride precursors have been used. This further emphasizes the need for a better wash solvent/washing technique. TEM images showed particles with average size <20 nm even after annealing at 500 °C and Pt and Cr were confirmed by the subsequent EDS analysis (Figure 7a and b).

The background material in seen in the TEM image could not be identified, but given the presence of Na detected in EDS, a sodium salt with organic materials might be present surrounding the particles. This matter is further discussed in a following section.

Pt−V. Vanadium is the most oxophilic of the metals used, and once again required the use of oxygen free precursors for products that contained significant amounts of V. Coreduction of VCl_2Cp_2 and $PtCl_2COD$ at room temperature in THF yielded a product with a Pt:V atomic ratio of 1:1 ± 5% by EDS, and pXRD showed relatively broad peaks with maxima shifted to higher angles compared to Pt. In an attempt to obtain the ordered PtV phase, the product was annealed at 1100 °C,

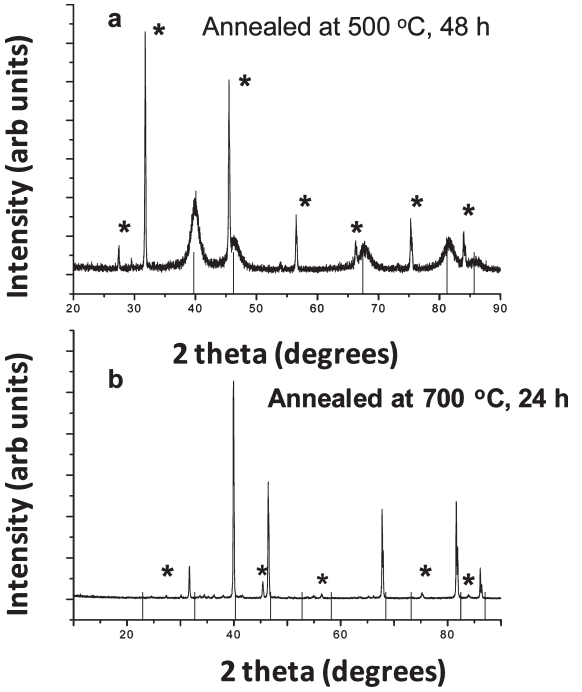

Figure 6. pXRD patterns of the $PtCl_2COD$ and $CrCl_3$ reduction reaction annealed at different temperatures. (a) Peaks with maxima close to the pure Pt phase (PDF no. 04-001-2683), but shifted (especially at higher angles) suggesting alloying of Cr into the Pt phase. (b) Ordered Pt_3Cr phase. The shifting of peaks might be due to compositional variation (the Pt−Cr phase diagram shows that the Pt_3Cr phase can have significant compositional width). The ordered Pt_3Cr phase was obtained only from annealing at 700 °C. Tick marks represent the known peak positions for Pt_3Cr (PDF no. 04-003-3551). * indicates the NaCl peaks.

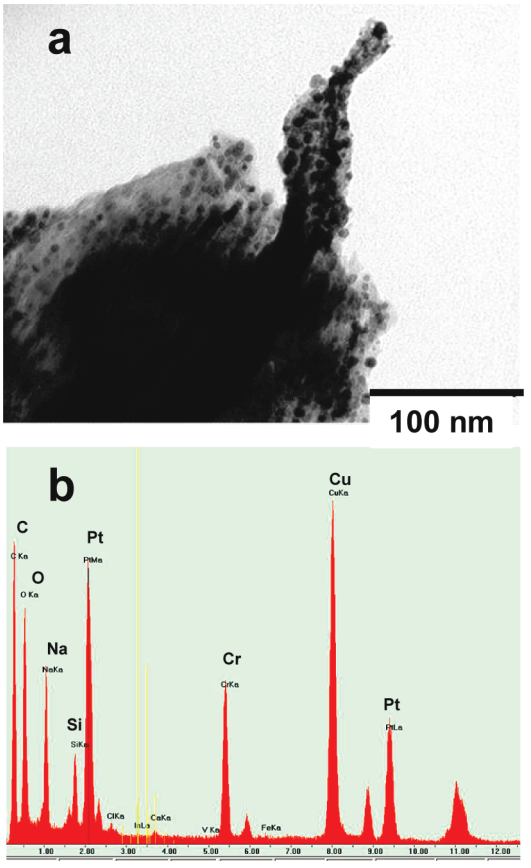

Figure 7. (a) TEM image of Pt−Cr particles from coreduction of $PtCl_2COD$ and $CrCl_3$, annealed at 500 °C for 48 h. (b) EDS spectra of this region. The Cu signal comes from the TEM grid; other impurities are also detected in minor amounts which might be from contamination from the TEM sample holder. The Na and C seen in the EDS spectrum are attributed to the background material seen in part a which are unidentified sodium and organics known to be present in the samples.

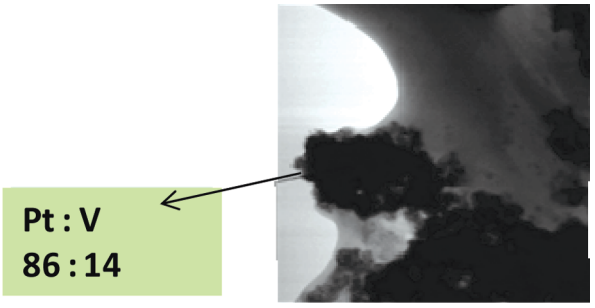

Figure 8. TEM image of Pt−V particles from coreduction of VCl_3THF_3 and $PtCl_2COD$ (full scale = 1300 nm). The inset shows composition data from EDS.

24 h, however, ordering peaks were not observed in the pXRD. At this temperature, there is significant attack of the silica tube, presumably by the V. Room temperature coreduction of VCl_3THF_3 with $PtCl_2COD$ yields a Pt:V atomic ratio of 3:1 (EDS). The decline in the amount of vanadium retained in the final product on moving to a precursor containing oxygen (VCl_3THF_3 vs VCl_2Cp_2) was at this point expected. pXRD showed broader peaks with maxima close to cubic Pt. The product was annealed in silica tubes sealed under vacuum to 700 °C for 4 h and 750 °C for 24 h in efforts to obtain an ordered Pt−V phase. EDS analysis using the nanoprobe mode in the TEM microscope on individual particles showed the Pt:V ratio to be close to 5:1 (Figure 8). This suggests the presence of the rest of the vanadium (as observed from EDS on broader regions) as a second phase, perhaps partially oxidized or closely associated with an oxygen containing contaminant species, and thus unable to form Pt−V species. This might be the reason why ordered phases are not always observed on annealing in spite of observing the right ratio of the required elements by EDS in large sample areas (1 μm square). The last reaction tried in the Pt−V system was a coreduction of VCl_3 and $PtCl_2COD$. Not unexpectedly, the Pt:V atomic ratio in the product was shown to be 1:1 by EDS. The product was annealed at 750 °C for 24 h and showed an ordered Pt_3V cubic phase with domain size of 41 nm (from the Scherrer equation). The X-ray diffraction peaks were slightly shifted from those reported, perhaps due to compositional width over which the Pt_3V is known to exist.[36] The compositions of the as prepared and annealed products indicate a loss of V as a solid impurity phase or phases that are not soluble in methanol.

Pt−Mn. Mn is intermediate between Ni and Cr in its oxophilicity, determined by metal−oxygen bond enthalpy (Supporting Information Table S1). Once again, $Mn(acac)_3$ was chosen as the starting precursor. Coreduction of platinum and manganese acetylacetonates at room temperature proceeded in a similar manner to the other metals, but the product was harder to recover after

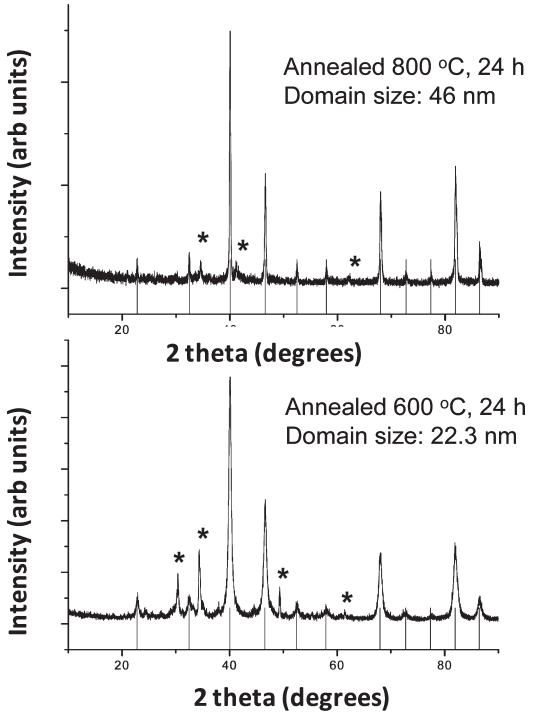

Figure 9. pXRD patterns of ordered Pt_3Mn nanoparticles obtained by coreduction of $Pt(acac)_2$ and $Mn(acac)_3$ followed by annealing at 800 and 600 °C, respectively. Tick marks represent the known peak positions for Pt_3Mn (PDF no. 03-065-3260). * denotes unknown impurity and/or NaCl peaks.

methanol/hexane washing. EDS showed the product composition to have a Pt:Mn atomic ratio of nearly 1:1. pXRD showed broad peaks with the maxima shifted from the pure Pt cubic phase, suggesting an alloy phase. An ordered Pt_3Mn phase was obtained on annealing the product in a tube sealed under vacuum (800 °C for 24 h, domain size 46 nm). Smaller particle sizes were also achieved by annealing at 600 °C for 24 h, having a domain size 22.3 nm (Figure 9).

These observations suggest the formation of an insoluble Mn impurity phase that is nonreactive with Pt. The presence of minor impurities was observed in both cases; however, contrary to expectations, the impurity peaks did not index to any known manganese oxide compounds.

Note that annealing any of the Pt−M phases with M = Ni through Mn, with the exception of Pt−Cu, resulted in black films deposited on the internal surface of the silica tubes. The film likely resulted from the decomposition of organic materials present in the product. TGA of the products also showed significant weight loss (30%) consistent with loss or decomposition of organic components in the reduced products. Such a weight loss translates to at least 3 C atoms per metal atom. This large value is consistent with the proposed dendridic nature of the unannealed nanoparticles and the inclusion of organic species inside the particle as well as on its surface. For Pt−Cu, annealing to high temperatures (higher than 400 °C), was not necessary, since the well-crystallized ordered PtCu phase could be obtained by annealing at 400 °C.

Selection of Precursors. In previous unpublished work in the group, it was observed that due to the high oxophilicity of the early transition metals, the presence of oxygen containing anionic or neutral ligands (e.g., $Pt(acac)_2$ or $Ti(THF)_4Cl_2$) often resulted in products containing oxygen while precursors such as $PtCODCl_2$ or $TiCp_2Cl_2$ produced cleaner products. Additionally, in the latter case (oxygen free precursors), the amount of Ti detected by EDS was higher (Pt:Ti 1:1) compared to the former (Pt:Ti 8:1). We hypothesize that the oxygen containing species from precursors bind strongly to the reduced oxophilic metal particles, such as Ti^0, rendering the metal labile to chemical attack by methanol or by eventual reaction with the THF itself, resulting in re-oxidation of the Ti and possible dissolution in methanol. This leaches out Ti from the very small particles produced by room temperature reduction, so it is unavailable to bind with Pt. This made it difficult to reproducibly obtain ordered Pt−Ti phases or even alloys with the desired Ti content. Reactions containing Cr, V, and Mn were more reproducible, as expected from their more positive reduction potentials and lower oxophilicity (Supporting Information Table S1). However, 1:1 ordered phases could not be obtained for these three metals. Hence, avoiding oxygen in the precursors is desirable for these elements. The results discussed in the above sections confirm this. Higher contents of the second element (Cr and V) in the end product were obtained from the coreductions of the respective metal chlorides and $PtCODCl_2$ than from the coreductions of $Pt(acac)_2$ and the metal acetylacetonate precursors. However, as the oxophilicity of the metal decreased on going from Ti to Mn, it became easier to obtain the alloy and intermetallic products with acetylacetonate precursors. While the product from Pt:Mn precursor ratio 1:1 indicated a composition of Pt:Mn 1:1 by EDS, the ordered phase obtained on annealing was Pt_3Mn. This strongly suggests that, although Mn was not removed during the workup process, about 65% of the Mn is unavailable for reaction with Pt. That Mn is likely oxidized by reaction with the precursor ligands, reaction or wash solvents, or with air. Given the much lower reactivity of oxygen with Cu, reactions with acetylacetonate precursors yielded products with 1:1 Pt:Cu ratio and PtCu ordered phases on annealing. In this case, no Cu was lost or oxidized in the process. Indeed, the ordered phase could be obtained at a lower temperature than for any of the other 3d metals examined.

Thus, precursor selection based on the guidelines discussed in this paper is vital for achieving the desired product phases. Up to Mn (in the order of increasing oxophilicity), oxygen containing precursors meeting other (solubility and oxidation state) criteria can be used. At Mn and beyond, chlorides and alkyl chlorides are by far better precursors for both metals, if significant alloying is desired. It needs to be mentioned here that for these studies, only commercially available precursors were used since the goal was to look at as many different metals as possible and to discover general principles and guidelines. Once the desirable properties for the precursors have been

Table 2. Summary of Precursors Selected for Different Metals Based on Desired Criterion and Final Composition of Products Obtained As a Result

second metal	precursor used for the second metal	Is the precursor oxygen free?	solubility in THF	Is the metal at its highest (or high) oxidation state?	Pt:X by EDS (where X is V, Cr, Mn, Ni, or Cu)
v	$V(Cp)_2Cl_2$	yes	ok	yes	1:1
	VCl_3	yes	poor	yes	1:1[a]
	$V(THF)_3Cl_3$	no	good	yes	3:1
Cr	$CrCl_3$	yes	poor	yes	1:0.8[a,b]
	$Cr(acac)_3$	no	excellent	yes	8:1
	Cr(ethylhexanoate)$_3$	no	good	yes	ND[c]
Mn	$MnCl_3$	yes	poor	yes	ND
	$Mn(acac)_3$	no	excellent	yes	1:1[a,b]
	Mn(ethylhexanoate)$_3$	no	good	yes	ND
Ni	$Ni(acac)_2$	no	excellent	N/A	0.6:1[a,b,c]
Cu	$Cu(acac)_2$	no	excellent	N/A	1:1[a]

[a] Ordered phase achieved. [b] C supported reactions explored. [c] Higher temperature reactions explored, ND stands for not done yet. Cr and Mn ethylhexanoate precursor reactions were not completely analyzed as the precursors come commercially as solutions in hexane and were difficult to purify and handle.

outlined, one may be able to synthesize even more appropriate ligands for the metals if they are not commercially available. A quick summary of precursor choice and related observations is given in Table 2.

Looking into the Contaminants, the Role of Na. As mentioned in the above sections, obtaining a well crystallized nanoparticle product with controllable diameters (5 to 15 nm) was not possible from room temperature reactions. Multiple washes and the use of methanol reduced, but did not eliminate, the contaminants and often resulted in product loss. Before high temperature annealing, low index peaks attributable to byproduct are observed in the pXRD.

Rarely could these peaks be indexed to known salts or oxides. EDS analyses always showed the presence of sodium in the final products. These observations strongly suggest that sodium is present in close association with some organic anion that is bound in or on the nanoparticles, increasing their polarity. This is consistent with the observed difficulty in precipitating the products out of even weakly polar solvents. Such a surface contamination would also significantly hinder particle growth through agglomeration and interdiffusion, until sufficiently high annealing temperatures are used. Finally, products containing small (2 nm) particles with metal−metal bonds that form a percolation network which includes organic ligands would likely be highly reactive.

Most of the metal atoms in such percolation structures would then be accessible to reactive solvents such as methanol. Thus, the more oxophilic of these metals reacted with and were leached out of the product when washed with methanol. If annealed before washing with methanol, larger particles were obtained even when decomposition of the included organic species was apparent. Once larger, crystallized nanoparticles are obtained, we would expect that the reactive metal would only be removed from the top few monolayers of the product, as is observed in typical dealloying experiments in bulk or thin film samples.[28,30,39]

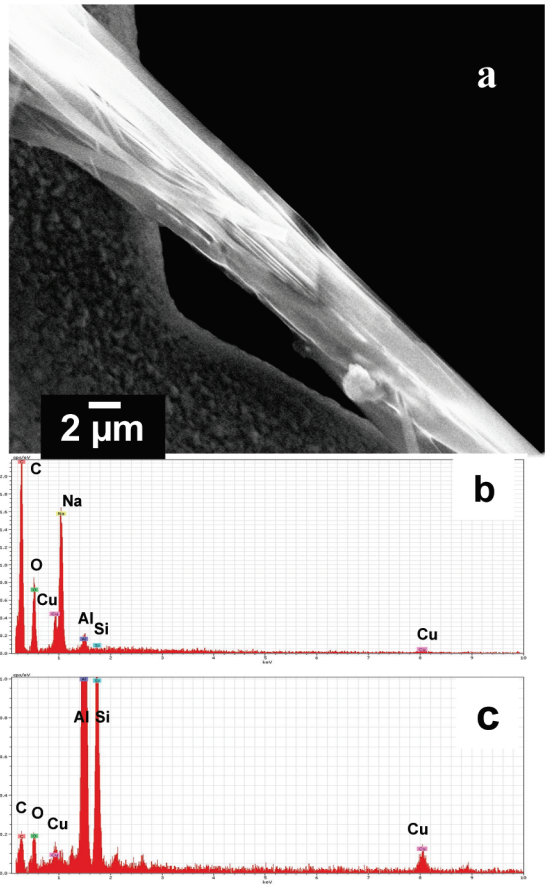

Figure 10. (a) STEM image of needlelike structures observed in the $PtCl_2COD$ and VCl_3 co- reduction. (b) EDS spectra obtained right on the needle. (c) EDS spectra of the immediate background. Although quantification of C is not possible by EDS measurements, the huge difference in the total count for C observed between the two cases suggests that a significant amount of carbon is present in the former region.

Considerable support for this hypothesis was obtained from STEM analyses of the nanoparticle samples. In the particular case for the Pt−V reaction with VCl_3 as the precursor, needlelike structures could be identified which were shown by EDS to contain only sodium and carbon (lighter elements could not be detected—Figure 10a and b). A background spectra obtained in the immediate vicinity showed much less carbon and no sodium

(39) Gregoire, J. M.; Kostylev, M.; Tague, M. E.; Mutolo, P. F.; van Dover, R. B.; DiSalvo, F. J.; Abruna, H. D. *J. Electrochem. Soc.* **2009**, *156*, B160–B166.

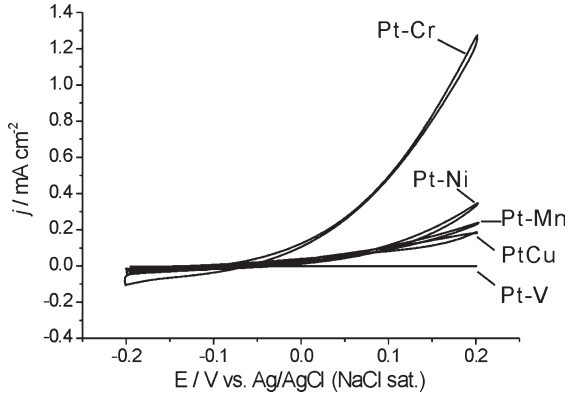

Figure 11. Rotating disk voltammograms for formic acid oxidation on PtCu, Pt−Ni, Pt−Cr, Pt−V, and Pt−Mn nanoparticles, as labeled. All data measured in a 0.5 M formic acid, 0.1 M sulfuric acid solution (electrode rotation rate 2000 rpm, potential scan rate 10 mV s^{-1}).

(Figure 10c). The identification of these sodium species suggest the possibility that if these were not present, much lower annealing temperatures would be needed to prepare the desired phases and loss of the reactive metal could also be prevented or reduced. Multiple washes with water followed by composition analyses showed that the sodium could be removed by water. However, water wash (especially on unannealed samples) causes complete oxidation of the reactive metals. Hence a balance needs to be found between choosing the appropriate ligands, reducing agent and the washing and annealing steps, to obtain the desired phase at low annealing temperatures or perhaps even at room temperature.

Electrocatalytic Activity. Figure 11 shows the rotating disk electrode voltammograms for formic acid oxidation on five different nanoparticle catalyst electrodes: PtCu, Pt−Ni, Pt−Cr, Pt−V, and Pt−Mn.

First, we discuss the activity of the unannealed nanoparticles. In comparing the relative activity of these electrocatalysts, two parameters are of significance: the onset potential for measurable oxidation of fuel and the oxidation current density at a given potential positive of onset. Thermodynamically, the onset potential of formic acid oxidation should occur near −0.2 V (vs an NaCl saturated Ag/AgCl electrode). Good catalysts are those with low overpotentials for oxidation, so that high oxidation currents occur at potentials only slightly more positive than −0.2 V. Therefore, the higher the current density at a given overpotential, the better the catalyst. For formic acid oxidation, Pt−Cu, Pt−Ni, Pt−Cr, and Pt−Mn exhibit reasonable electrocatalytic activity, while Pt−V is almost inactive (Table 3). In addition to the onset potentials, Table 3 also lists the current densities (in units of milliamps per centimeter of catalyst surface, a surface area determined by BET) of the five catalysts at four specific potentials.

This current density is a direct measure of electrocatalytic efficiency. In this study, all the electrocatalyst materials examined had different particle sizes and, consequently, different surface areas and specific surface areas. Furthermore, electrochemical protocols for the measurement of the specific surface area for these novel

Table 3. Onset Potentials and Current Densities at Different Voltages for PtCu, Pt−Ni, Pt−Cr, Pt−V, and Pt−Mn Nanoparticles for Formic Acid Oxidation[a]

		current density (mA cm^{-2})			
catalyst	onset potential (mV)	−100 mV	0 mV	+100 mV	+200 mV
Pt−Cr	−100	0.001	0.124	0.503	1.272
Pt−Ni	−40	0	0.018	0.115	0.347
Pt−Mn	−100	0.004	0.036	0.108	0.238
PtCu	−100	0.005	0.039	0.082	0.187
Pt−V	200	0	0	0	0.001
Pt black[b]	0	0	0.003	0.018	0.05

[a] All specified potentials are vs Ag/AgCl (NaCl sat). [b] For Pt black, see ref 16.

intermetallic nanoparticles have not been established. This is in contrast to Pt, for which methods are well-established (e.g., Coulombic integration of hydrogen adsorption). To make the most-meaningful comparison of the raw current data collected, we normalized currents to the measured BET surface area of the respective catalysts. The resulting surface area normalized current densities appear in plots and in the table as milliamps per squared centimeter (where the squared centimeter measurement is the BET surface area for the catalyst coated on the GC electrode). From the values presented in Table 3, for formic acid oxidation, it is evident that PtCu, Pt−Ni, Pt−Cr, and Pt−Mn have activities that are far superior to that of Pt black. Pt−Cr, in particular, exhibits a current density that is much higher (> 20 times) than Pt black,[16] the commercially available electrocatalyst.

The electrochemical activities discussed above are for the unannealed products. The annealed phases were always found to have very little electrochemical activity, presumably due to decomposed carbonaceous materials covering the surface of the nanomaterials. Except for Pt−Cu, all Pt−M products were annealed at temperatures higher than 400 °C in order to obtain ordered phases, and black coatings were found on the walls of the tubes in which these products were annealed. Annealing Pt−Cu was carried out at 400 °C or less, since by 250 °C large, well crystallized (14 nm) intermetallic particles are already attained. Even after annealing at 400 °C, no black film was observed for the ordered PtCu samples. Because of this, we were hopeful that the ordered phase would have enhanced activity due to the lack of decomposed carbonaceous material on the surface, but the electrochemical data for PtCu sample still showed a decrease in activity per square cm of catalyst surface area. Therefore, all the data presented in Figure 11 and Table 3 are only from the unannealed samples.

Conclusions

Through the above synthetic explorations, we have been able to understand and control several key factors in achieving the alloy and intermetallic phases for a wide range of metals from Cu to V. The oxophilicity of the metal, and the composition of the ligands and solvents (especially the presence of oxygen) are very important in determining the composition of the products. Starting

with Pt:M 1:1 precursors in all cases, the final phases obtained could contain less M due to loss of the reactive metal. For example, while we could obtain ordered PtCu and PtNi nanoparticles by annealing, only Pt_3Mn and Pt_3V could be similarly obtained. Mn and V are more oxophilic than Cu or Ni, and some of the Mn and V reacts with methanol or other species so that it is not available to react with the Pt even under annealing conditions. With more oxophilic metals, like vanadium, even the use of VCl_3THF_3 as a reactant resulted in smaller V inclusion, presumably V(0) reacts with the THF and that product is easily washed away by polar solvents like THF and methanol. The same appears to be true for chromium, but to a smaller extent (less Cr is lost than V as seen by EDS and in the final composition of the annealed products). In the end, the balance between having clean surfaces of the metal species in the system (washes) and mixing them well/promoting diffusion while their surface is clean (perhaps including in situ heating and stirring/annealing) after the precursors are reduced is vital for the nanoparticles to grow and order.

In a poorly crystallized, product containing organics in a percolation network of metal−metal bonds, the more reactive metal is vulnerable to be removed by reaction with the washing solvents or oxidized on the subsequent exposure to air. Further, such products usually fail to precipitate out of the reaction/wash solvent. When these particles are isolated by evaporation of the solvent, the product is a highly agglomerated, low surface area substance. On the other hand, well crystallized nanoparticles with sizes greater than about 5 nm can only form by excluding organics from the interior of the particle. There could of course still be some surface contamination, but such particles appear to be much less reactive with methanol or air.

Further optimization of processing conditions is required in order to synthesize the materials at lower temperature and to reliably produce smaller nanoparticles (in the 5−10 nm range). But the activity observed in the low surface area products shows the underlying catalytic potential that can be reached if these nanophases can be synthesized as cleaner, small particle size materials. The presence of sodium and organics in the unannealed products is clear. If we can find reactants and conditions that eliminate such contamination, the products should be better crystallized, requiring either no annealing or annealing at lower temperatures. We are continuing these studies to see if such conditions can be found for Pt−M couples beyond PtPb and PtCu.

In spite of the challenges remaining, our work here has provided a route for obtaining nanometer sized alloys and intermetallics of Pt with very reactive metals which are active catalysts for formic acid oxidation. Also, identifying, understanding, and outlining the key issues is the first step that will hopefully lead to higher yield synthetic schemes producing nanoparticles with higher activity and stability.

Acknowledgment. This work was supported by the Basic Energy Sciences Division of the Department of Energy. The authors thank Mick Thomas for help with the UHV-STEM data acquisition and analysis, John Hunt for the same for the EPMA microprobe, and John Grazul with the TEM. All of these tools are managed and maintained by the Cornell Center for Materials Research (CCMR), an NSF supported MRSEC through grant DMR-0520404.

Supporting Information Available: Some further discussion and more figures and tables. This information is available free of charge via the Internet at http://pubs.acs.org/.